This is the peer reviewed author accepted manuscript (post print) version of a published work that appeared in final form in:

Oppong, Francis, Zhongyang, Luo, Li, Xiaolu, Song, Yang, Xu, Cangsu, Lacina Diaby, Abdullatif 2022 'Methyl pentanoate laminar burning characteristics: experimental and numerical analysis', Renewable Energy, vol. 197, pp. 228-236

This output may not exactly replicate the final published authoritative version for which the publisher owns copyright. It is not the copy of record. This output may be used for non-commercial purposes. This version is licensed under a Creative Commons CC-BY-NC-ND 4.0 license (http://creativecommons.org/licenses/by-nc-nd/4.0/).

The final definitive published version (version of record) is available at: https://doi.org/10.1016/j.renene.2022.07.127

Persistent link to the UniSA Research Outputs Repository: https://researchoutputs.unisa.edu.au/11541.2/30335

General Rights

Copyright and moral rights for the publications made accessible in the UniSA Research Outputs Repository are retained by the authors and/or other copyright owners and it is a condition of accessing publications that users recognize and abide by the legal requirements associated with these rights.

- Users may download and print one copy for the purpose of private study or research.
- You may not further distribute the material or use it for any profit-making activity or commercial gain
- You may freely distribute the persistent link identifying the publication in the UniSA Research Outputs Repository

If you believe that this document breaches copyright, please contact us and provide details. We will remove access to the work immediately and investigate your claim.

Methyl pentanoate laminar burning characteristics: Experimental and numerical analysis

Francis Oppong[a], Luo Zhongyang[a], Xiaolu Li[b], Yang Song[c], Cangsu Xu[a*], Abdullatif Lacina Diaby[d]

[a]College of Energy Engineering, State Key Laboratory of Clean Energy Utilization, Zhejiang University, Hangzhou, 310027, China P.R.

[b]College of Mechanical and Electrical Engineering, China Jiliang University, Hangzhou, 310018, China P.R.

[c]Zhejiang Tongji Science and Technology Career Academy, Hangzhou, 311231, China P.R.

[d]UniSA Online (STEM), University of South Australia, Adelaide, SA 5000, Australia.

*Corresponding author: xucangsu@zju.edu.cn

Abstract

This study investigated the laminar combustion characteristics of methyl pentanoate (MPe) using the constant volume combustion chamber at the initial pressures and temperatures of 1, 2 and 4 bar and 423, 453 and 483 K respectively over the equivalence ratios ranging from 0.7-1.4. The experimental and simulated peak pressures showed a good trend irrespective of the disparities between both results. The experimental laminar burning velocities agreed well with the simulated laminar burning velocities. Also, laminar burning velocities at the initial temperatures and pressures up to 573 K and 8 bar respectively were estimated using a deduced empirical formula. Last but not least, the main pathways for the decomposition of MPe were MPe→MPe2J→MPeMJ→MPe3J.

Keywords: Methyl pentanoate; Laminar burning velocity; Peak pressure; Pressure rise rate

1. Introduction

Greenhouse gas (GHG) is the main cause of global warming which has recently become a thorny issue. In light of this, climate change conferences like the Paris Agreement (Conference of the Parties (COP21)) and the most recent COP26 meeting held in Glasgow aimed at reducing carbon dioxide and other pollutant emissions into the atmosphere to keep global warming at 2°C or 1.5°C. Moreover, China aims to reach a carbon dioxide peak before 2030 and attain net-zero carbon dioxide before 2060. The EU also intends to achieve net-zero carbon dioxide before 2050 to have low carbon development.

Renewable green energies could be used to achieve these emission reduction targets to attain carbon dioxide neutrality and a low carbon economy [1–3]. Methyl pentanoate (MPe) is a typical example of green fuel which could be used to reduce GHG in the atmosphere [4,5]. MPe is produced from low-grade biomass resources or lignocellulose via levulinic acid (LVA) or γ-valeralactone (gVL) [6,7]. Besides, MPe has been considered a drop-in fuel or fuel additive in internal combustion engines (ICEs) and could increase ICEs efficiency [8,9]. Due to MPe's suitability as fuel in ICEs, Contino and co-researchers [9] investigated the engine performance and emissions of MPe and its blend (20%) with primary reference fuel (PRF95) in a spark-ignition engine (SI) engine. MPe flames propagated faster than PRF95. The study revealed that MPe knocking resistance was higher than that of PRF95. Elsewhere, Contino et al. [8] studied the combustion characteristics of MPe in the HCCI engine and asserted that the autoignition reactivity span of MPe was high. Using experiments and kinetic modelling, Korobeinichev and collaborators [10] studied the combustion intermediates of MPe and argued that the experimental data and the kinetic model results agreed well. Gerasimov et al. [11] proposed a mechanism consisting of 92 species and 330 reactions to investigate the extinction rate and ignition delay times (IDTs) of MPe. Although the simulated IDTs were lower than the experimental IDTs they had a good trend. Furthermore, Weber and co-workers studied the IDTs of MPe at 15 and 30 bar, 720 to 800 K, and the equivalence ratios of 0.25 to 2.0 [12]. The IDTs exhibited two-stage ignition at 720-760 K and 740-760 K for 15 bar and 30 bar, respectively. The IDTs also showed a negative temperature coefficient (NTC) at 720-800 K, a pressure of 15 bar and equivalence ratio of 2.0, and a pressure of 30 bar and an equivalence ratio of 1.0. In a different research, Pengfei et al. [13] studied the IDTs of MPe over reflected shock waves at the temperatures of 1050-1350 K, pressures of 1.5 and 16 bar using the equivalence ratios of 0.5, 1.0, and 2.0 for MPe/air and 1210-1410 K, 3.5-7 bar and equivalence ratios of 0.75 and 1.25 for MPe/4%O_2/Ar. The IDTs of MPe/4%O_2/Ar were higher than that of MPe/air due to the higher concentration of MPe/4%O_2/Ar.

Knyazkov et al. [14] evaluated the effect of MPe on n-heptane and showed that the addition of MPe to n-heptane reduced the fuel mixture flame temperature and combustion intermediates that produce polycyclic aromatic hydrocarbons (PAH). Finally, Shang et al. [15] reported that chain branching reactions MPe ⇔ $CH_3OC(=O)CH_3$ + CH_2CHCH_3 and MPe ⇔ $CH_3OC(=O)CH_2$ + $CH_2CH_2CH_3$ controlled the decomposition of MPe.

Apart from IDTs, combustion intermediates, etc., other combustion characteristics of paramount importance are the laminar burning velocity (LBV), peak pressure, pressure rise rate, etc. LBV could be used to determine the reactivity, diffusivity, combustion phasing, turbulent burning velocity, flame stability, extent of combustion emissions, and validate the chemical kinetic mechanisms of fuels [16–18]. Unfortunately, regardless of LBV relevance, the LBV of MPe has not been extensively studied, except for Contino et al. [9] and Gerasimov et al. [11] papers that reported MPe LBVs at 423 K (1 and 3 bar and equivalence ratios of 0.8-1.4) and 363 K (1 bar and equivalence ratios of 0.66-1.54), respectively. Similarly, the peak pressure and pressure rise rate could be used to examine combustion devices' performance but no studies have reported the peak pressures and pressure rise rates of MPe. In the framework of this significance, the main objective of this study is to evaluate the LBV of MPe at elevated pressures (1, 2, and 4 bar) and temperatures (423, 453, and 483 K) over a wide range of equivalence ratios of 0.7-1.4 using experimental and numerical analysis. The constant volume method (CVM) of the spherically expanding flame method is used to determine the LBV of MPe. Also, the peak pressures and pressure rise rates of MPe are presented and discussed. The reaction pathways of MPe combustion are presented and discussed. The originality of this study is that it provides comprehensive combustion characteristics of MPe at elevated pressures and temperatures which have not been reported in the literature. Moreover, this study proposes empirical formula which can be used to estimate the laminar burning velocity of MPe at elevated pressures and temperatures. In summation, this study provides detailed information on the combustion science of MPe which could be used as the framework for more research on MPe towards its practical applications in ICEs.

2. Experimental and numerical investigations

The experimental setup used to investigate the combustion characteristics of MPe in this study could be found in the authors' previous works [16,19]. The experimental facility comprises a constant volume combustion chamber (CVCC) with an internal volume of 2.06 L formed by the cross-intersection of three cylinders. A schlieren imaging system is used together with the CVCC to investigate MPe burning characteristics. The flame images of MPe combustion were recorded with a high-speed camera with a resolution of 515×515 and a filming speed of 12800

fps. A high accurate pressure gauge (± 0.05%) and sensors (0.001 Pa resolution) and K-type thermocouples (± 0.75%) were used to measure the experimental initial pressure, combustion pressure, and initial temperature respectively. Methyl pentanoate (purity 99.99%) was injected into the CVCC using micro syringes ranging up to 1mL. The injected fuel was allowed to vaporize for 5 minutes and mixed with pure compressed air (99.99%) in the CVCC. The methyl pentanoate/air mixture in the CVCC was allowed to mix for 3 minutes (form a homogeneous mixture) before ignition. After each experiment, a vacuum pump was used to clean burnt gas in the CVCC. The initial pressures (p_0) of 1, 2 and 4 bar, initial temperatures (T_0) of 423, 453 and 483 K and equivalence ratios (ϕ) of 0.7-1.4 (interval = 0.1) were used in this experiment.

Herein, the uncertainty of the experiment was determined using the root mean square method $\sqrt{\Delta U_T^2 + \Delta U_p^2 + \Delta U_F^2 + \Delta U_V^2}$ [20], which was < 5%. ΔU_T^2, ΔU_p^2, ΔU_F^2, and ΔU_V^2 are the uncertainties of the initial temperature, initial pressure, fuel measurement, and CVCC volume respectively. The uncertainties are respectively given as 0.75%, 0.15%, 3.28%, 0.7%. For each equivalence ratio, the experiment was performed at least three times for repeatability and reproducibility, to ensure 90-95% certainty of the experiment data and also to reduce random uncertainties in the experiment. The average of the three datasets was used as the final data. Moreover, the 95% confidence interval is used to present the experimental errors in the data to deal with other environmental uncertainties which invisibly influenced the experiment.

On the one hand, the numerical analysis was performed using Cantera thermochemical software [21]. The methyl pentanoate chemical mechanism proposed by Gerasimov et al. [11] was used in Cantera to determine the laminar combustion characteristics of MPe/air mixtures. The 1D freely propagating flame code was used to calculate MPe/air mixtures laminar burning velocity. The laminar burning velocity was determined using computational criteria (width = 0.03 m, ratio = 3, slope = 0.06, and curve = 0.12). In Cantera, the computational grid width is automatically adapted to determine the accurate solution or to ensure convergence of the solution. The adiabatic flame model was used to determine MPe peak combustion pressures.

3. Data processing and analysis

The constant volume method (CVM) of the spherically expanding flame method was used to determine the laminar burning velocity. To determine the laminar burning velocity by the CVM, the pressure history (p) and the burnt mass fraction (x) of the combustion process have to be known. Therefore, the experimental pressure data were filtered and processed with Equation (1) to obtain the pressure and pressure rise rate curves (dp/dt) presented in

Figure 1a. The raw pressure data was filtered with the Gaussian filter. The filtering and processing of the pressure data were performed using 1D Python in-house code.

$$p = 0.49346(V - V_0) + p_0 \quad (1)$$

p_0, V and V_0 are the initial pressure, voltage and initial voltage of the pressure sensor readings on the oscilloscope respectively. Furthermore, the two-zone burnt mass fraction formula (Equation (2)) proposed by Luijten et al. [22] was used to determine the burnt mass fraction of MPe. The burnt mass fraction of MPe was put into Equation (5) to determine the stretched laminar burning speed (S_L) curve shown in Figure 1b. Equation (6) was used to extrapolate the unstretched laminar burning speed (S_L^0) at the initial conditions as shown in Figure 1b.

$$x = \frac{p - p_0 f(p)}{p_e - p_0 f(p)} \quad (2)$$

$$\frac{dx}{dp} = \frac{1 - p_0 f'(p)}{p_e - p_0 f(p)} + \frac{p_0 f'(p)[p - p_0 f(p)]}{[p_e - p_0 f(p)]^2} \quad (3)$$

$$p_0 f'(p) = \left(\frac{\gamma_u - \gamma_b}{\gamma_u}\right)\left(\frac{p}{p_0}\right)^{-1/\gamma_u} \quad (4)$$

The stretched laminar burning velocity (S_L) is calculated as [23]:

$$S_L = \frac{R_v}{3}\left(1 - (1 - x)\left(\frac{p_0}{p}\right)^{1/\gamma_u}\right)^{-2/3}\left(\frac{p_0}{p}\right)^{1/\gamma_u}\frac{dp}{dt}\frac{dx}{dp} \quad (5)$$

The unstretched laminar burning velocity (S_L^0) is computed as:

$$S_L = S_L^0\left(\frac{p}{p_0}\right)^{\beta} \quad (6)$$

p_e and R_v are the peak pressure and the vessel inner radius respectively whereas γ_u nad γ_b are the unburnt and burnt gases specific heat ratios respectively. β is the pressure coefficient. $p/p_0 \geq 1.5$ was used for the extrapolations of the laminar burning velocity considering stretch and heat loss in the combustion chamber [24,25].

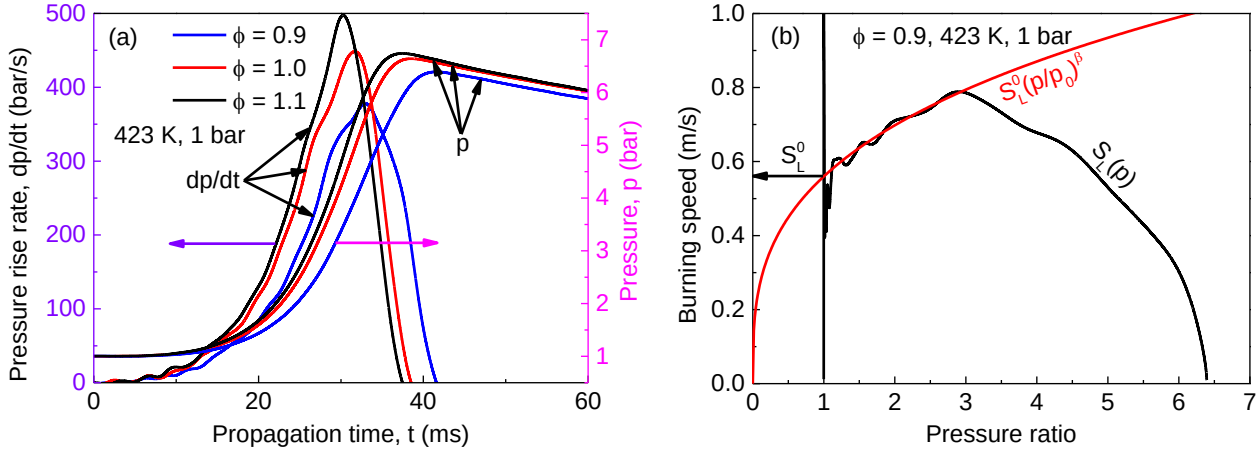


Figure 1. MPe/air mixtures (a) pressure and pressure rise rate curves and (b) burning velocity curve.

4. Results and discussion

4.1. Peak pressure and maximum pressure rise rate

The peak pressure of a combustible mixture describes the quantity of energy produced from the combustion of the fuel mixture. Therefore, the peak pressure could be used to evaluate the performance of combustion devices. Figures 2a and b plot MPe/air mixtures peak pressures at different initial pressures and temperatures. As provided in Figure 2a, the peak pressure increases with increasing initial pressures due to increased charge or mass of fuel in the combustion chamber and increased the total heat released [26,27]. Also, increased initial pressure can increase the kinetic energy or gas-particle collision of the combustion gases and enhance the chemical reaction leading to increased peak pressures [28]. The maximum peak pressure at 1 bar is 6.74 bar, 2 bar is 13.83 bar and 4 bar is 28.03 bar. In contrast, Figure 2b indicates that the peak pressure decreases with increasing initial temperature due to decreased charge in the combustion chamber leading to decreased total heat released [29,30]. The maximum peak pressure at 423 K is 6.74 bar, 453 K is 6.35 bar and 483 K is 5.90 bar. Figures 2a and b also compare the experimental peak pressures and simulated peak pressures. Although the experimental and simulated peak pressures have a consistent trend, the simulated peak pressures are higher than the experimental results due to heat loss in the combustion chamber during the experiment [31].

Furthermore, the maximum pressure rise rate embodies the build-up pressure of a combustion process and could be equally used to assess the performance of combustors. Figures 2c and d present MPe/air mixtures maximum pressure rise rates at different equivalence ratios and different initial pressures and temperatures respectively. The maximum pressure rise rate increases as the initial pressure increases due to the higher quantity of fuel and higher thermal energy released from MPe/air mixtures combustion [26,32]. The highest value of the maximum pressure rise rate at 1 bar is 497.43 bar/s, 2 bar is 953.09 bar/s and 4 bar is 1765.31 bar/s. Generally, the maximum pressure rise rate increases with decreasing initial temperatures as shown in Figure 2d. The highest maximum pressure rise rate at 423 K is 497.43 bar/s, 453 K is 490.35 bar/s and 483 K is 454.32 bar/s.

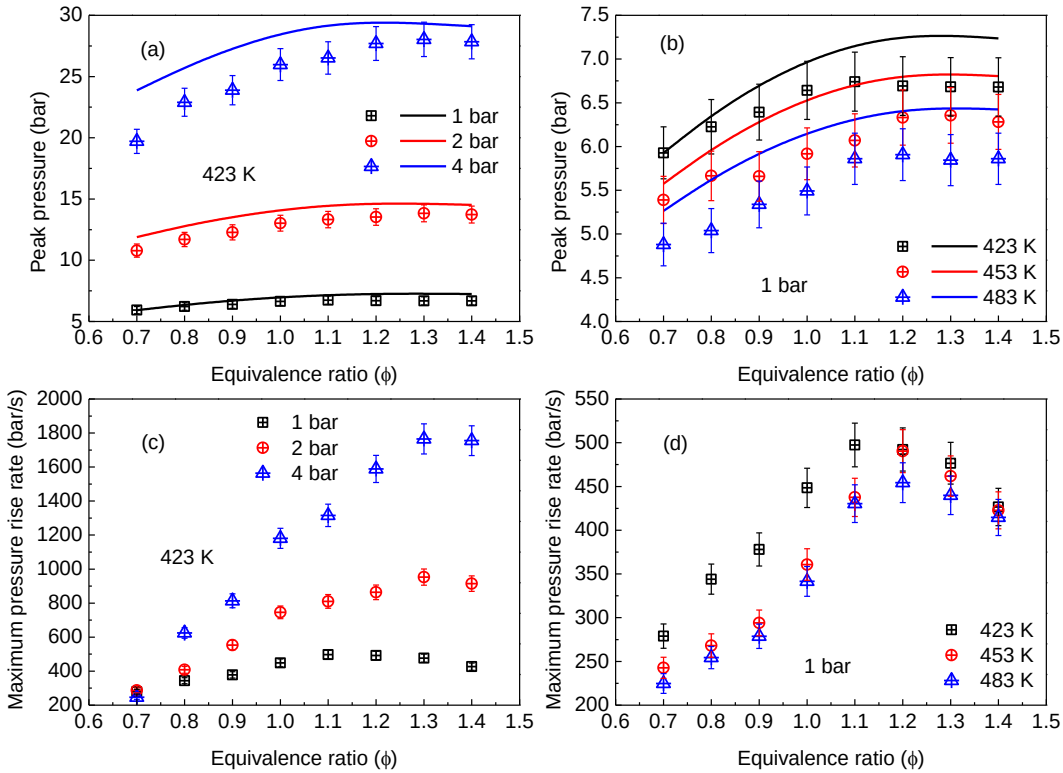


Figure 2. MPe/air mixtures (a)-(b) peak pressure and (c)-(d) maximum pressure rise rate.

4.2. Laminar burning velocity

Figure 3 compares the laminar burning velocities of MPe with the laminar burning velocities of gasoline (Hu et al. [33]), ethanol (Broustail et al. [34]), Isooctane (Contino et al. [9]), and n-butanol (Wang et al. [35]). MPe/air mixtures data are compared with the other fuels data to show the potential of MPe as a fuel in internal combustion engines. Figure 4 presents MPe/air mixtures laminar burning velocities at different pressures and temperatures. The laminar burning velocities were obtained by extrapolation at the initial conditions. In Figure 4a, this study's laminar

burning velocities are compared with MPe/air mixtures burning velocity data measured by Contino et al. [9]. This study's burning velocities exhibit a good trend with Contino et al's data. Moreover, from Figures 4a-c, the laminar burning velocities of MPe/air mixtures decrease with increasing initial pressures due to changes in two/three-body termination reactions and increased burnt gas density [36,37]. On the other hand, the plots show that the laminar burning velocities of MPe/air mixtures increase as the initial temperature increases owing to increased active radicals and adiabatic flame temperature of the combustion process [16,38]. Figures 4a-c also compare the measured experimental laminar burning velocities with laminar burning velocities computed with Gerasimov et al. [11] MPe/air mixtures chemical mechanism. The simulated results have a good tendency with the experimental data. As shown in Figure 4d, the simulated and experimental laminar burning velocities correlate well within ±10%. It is worth noting that the laminar burning velocities at 1.3 and 1.4 for 2 and 4 bar are not presented because they were influenced by flame instability.

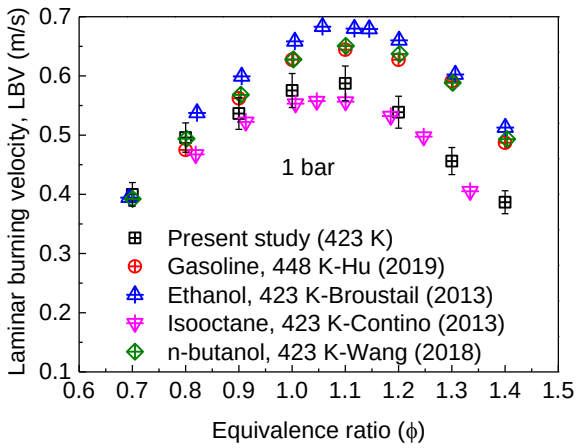


Figure 3. Comparison of MPe/air mixtures laminar burning velocities with different fuels laminar burning velocities.

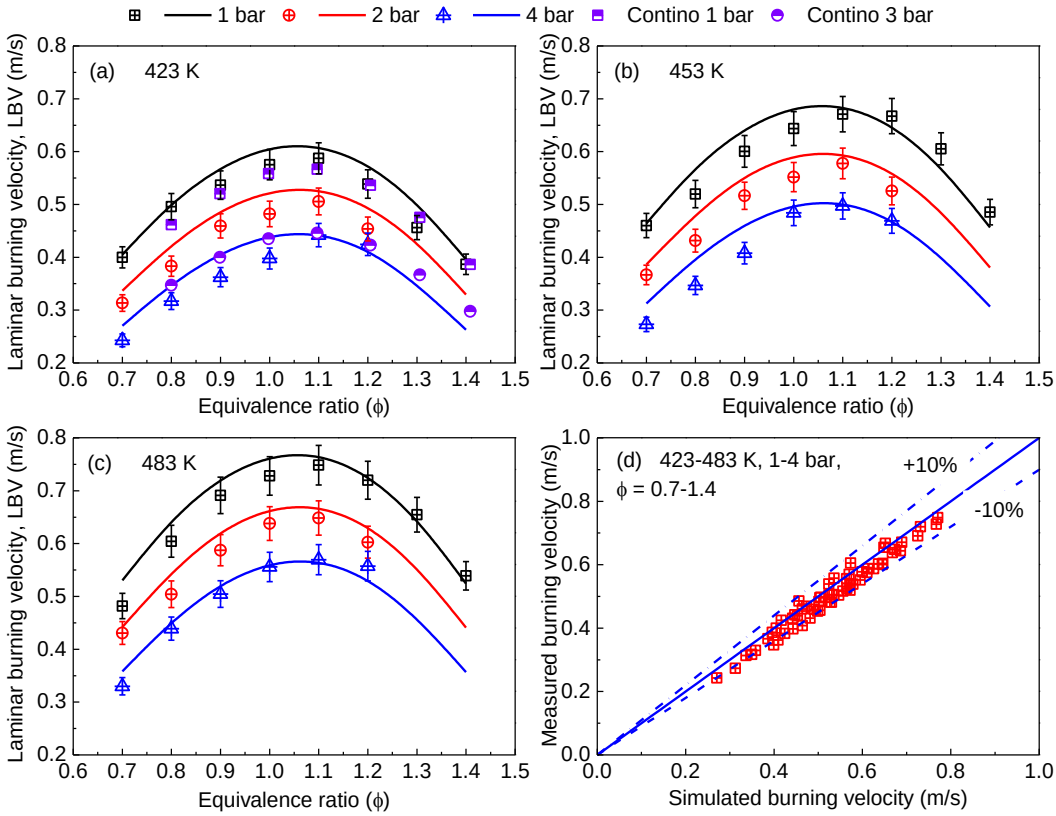


Figure 4. MPe/air mixtures extrapolated laminar burning velocities. (a)-(c) solid: simulations and symbols: experiments.

The experimental data at the initial temperature of 483 K and the initial pressures of 1, 2 and 4 bar were fitted to Equation (7) to obtain MPe/air mixtures laminar burning velocities at elevated pressures and temperatures up to 8 bar and 573 K respectively. Due to the observation of apparition of cellularity/instability at the equivalence ratios of 1.3 and 1.4 at the pressure of 2 and 4 bar, the data at the equivalence ratios of 1.3 and 1.4 for 1, 2, and 4 bar were excluded from the derivation of the empirical formula.

$$S_L = S_L^0 (p_r)^{\beta} (T_r)^{\alpha} \tag{7}$$

$$S_L^0 = -6.7185\phi^4 + 24.03\phi^3 - 33.577\phi^2 + 22.143\phi - 5.1487 \tag{8}$$

$$\beta = -0.6414\phi^2 + 1.8612\phi - 1.4071 \tag{9}$$

$$\alpha = 17.286\phi^2 - 34.232\phi + 18.65 \tag{10}$$

where $p_r = p_u/p_{ref}$ and $T_r = T_u/T_{ref}$. p_u and p_{ref} represent the unburnt gas pressure and reference pressure respectively. T_u and T_{ref} denote the unburnt gas temperature and reference temperature respectively. Here, p_{ref} and T_{ref} are 1 bar and 483 K respectively. The validity range for the proposed formula is $483 \leq T(K) \leq 573$ and $1 \leq p(bar) \leq 8$.

Figures 5a-c display the pressure coefficients (β), temperature coefficients (α) and the laminar burning velocity used for the empirical correlation. As depicted in Figure 5a, the pressure coefficients negatively impact the laminar burning velocity. This indicates that the laminar burning velocity decrease with increasing initial pressures. Conversely, Figure 5b reveals that the temperature coefficients have a positive influence on the laminar burning velocity. Therefore, the laminar burning velocity increase with increasing initial temperatures. Figures 6a-c present the proposed empirical formula laminar burning velocities up to the pressure and temperature of 8 bar and 573 K respectively. Even though there are discrepancies between the simulated and the empirical correlation results yet they are satisfactory. Therefore, the empirical formula could be tentatively used to determine the laminar burning velocity of MPe/air mixtures at elevated pressures and temperatures. Figures 6a-c disclose that the laminar burning velocities decrease with increasing initial pressures and increase with increasing initial temperatures.

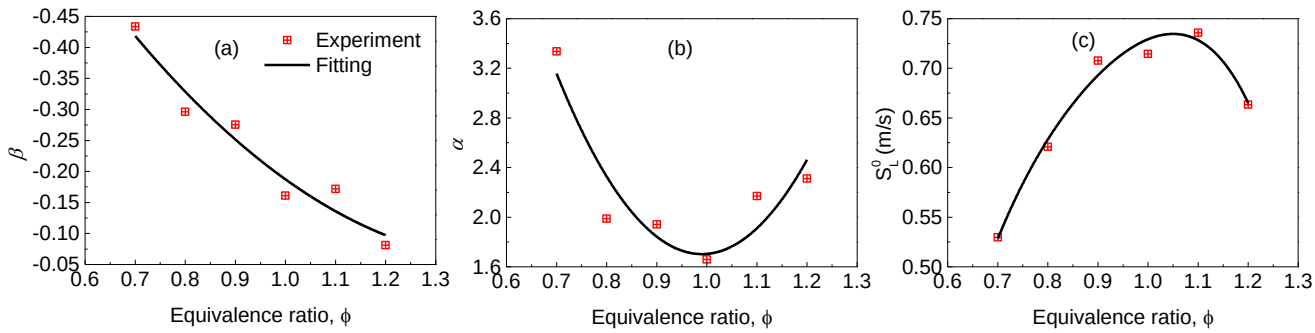


Figure 5. MPe (a) Pressure coefficients, (b) temperature coefficients and (c) laminar burning velocities.

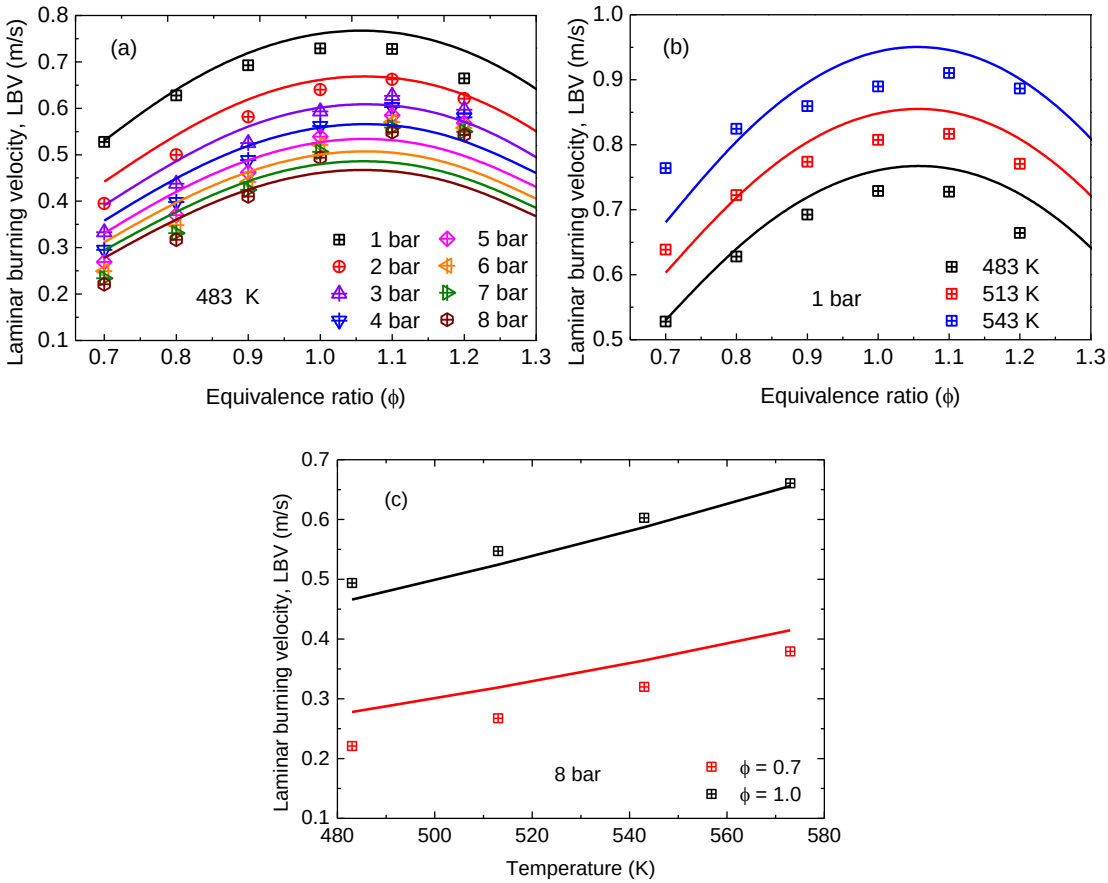


Figure 6. Laminar burning velocities at different (a) pressures and (b)-(c) temperatures obtained with the proposed empirical correlation. Symbols: empirical correlation data and Lines: simulation results.

4.3. Sensitivity analysis, progress rate, production rate, and reaction pathway

Figures 7a-c plot the chemical reactions at different equivalence ratios, initial pressures and initial temperatures. As seen in Figures 7a-c, the reactions R130: $H + O_2 \Leftrightarrow O + OH$, R134: $H_2 + OH \Leftrightarrow H + H_2O$, R146: $CO + OH \Leftrightarrow CO_2 + H$, R151: $HCO + M \Leftrightarrow CO + H + M$, and R284: $C_2H_3 + O_2 \Leftrightarrow CH_2CHO + O$ have a positive influence on the combustion of MPe and expedite the reactivity of MPe. Amongst these reactivity promoting reactions, the chain branching reaction R130: $H + O_2 \Leftrightarrow O + OH$ immensely accelerates the reactivity and increases the flame speed/burning velocity. Thus, R130: $H + O_2 \Leftrightarrow O + OH$ produces a lot of O and OH radicals which increases MPe reactivity and accelerates MPe flame speed. Conversely, the reactions R131: $H + O_2 + M \Leftrightarrow HO_2 + M$, R132: $H + OH + M \Leftrightarrow H_2O + M$, R158: $CH_4 (+M) \Leftrightarrow CH_3 + H (+M)$, R167: $2CH_3 \Leftrightarrow C_2H_5 + H$, and R254: $C_3H_6 + OH \Leftrightarrow C_3H_5\text{-}A + H_2O$ have adverse influence on the combustion of MPe. They exterminate the production of active radicals in the combustion process and inhibit the reactivity of MPe, therefore, decreasing the flame speed. However, the

three-body chain termination reactions R131: H + O_2 + M ⇔ HO_2 + M and R132: H + OH + M ⇔ H_2O + M significantly obstruct the reactivity of MPe combustion.

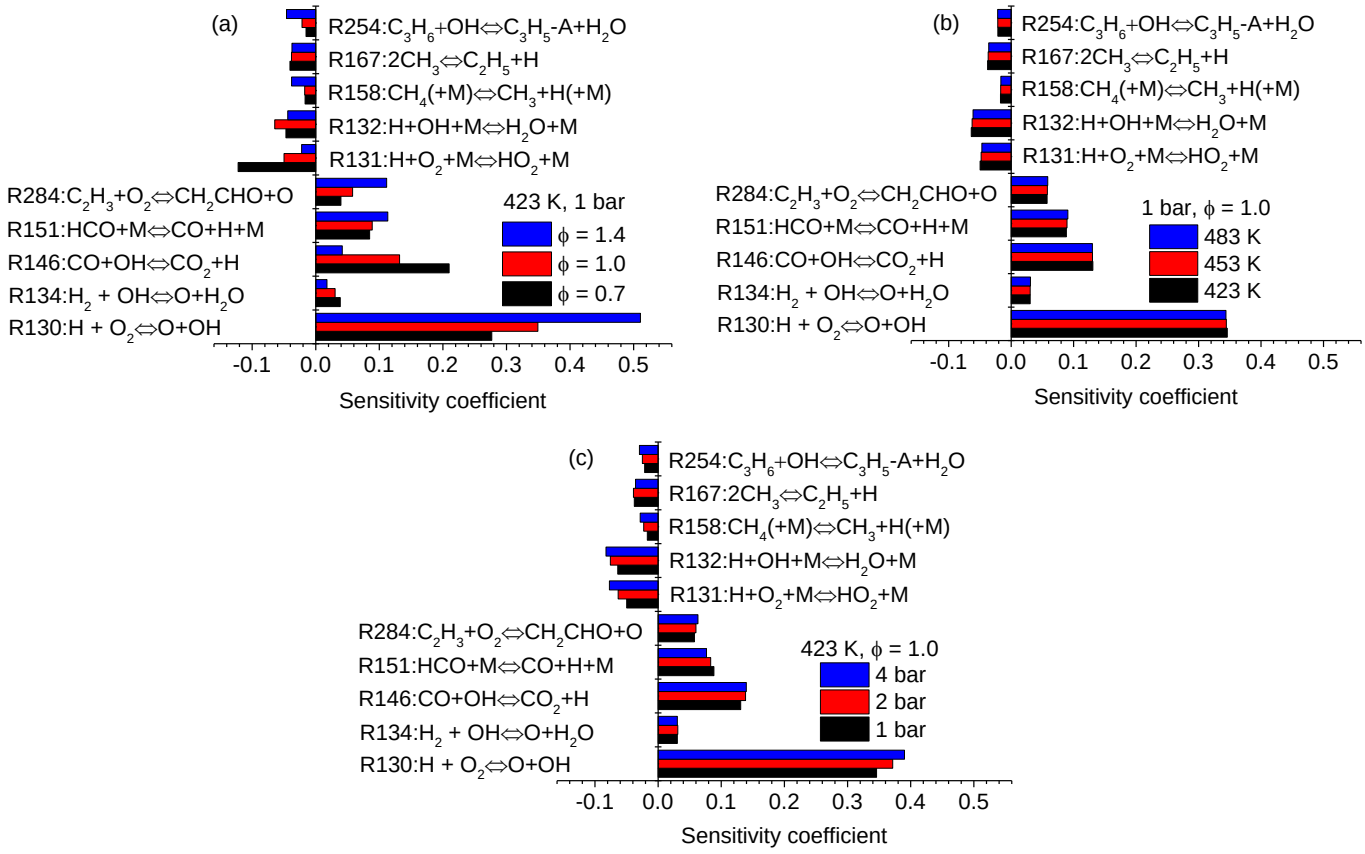


Figure 7. MPe laminar burning velocity sensitivity coefficients at different (a) equivalence ratios, (b) temperatures and (c) pressures.

Figures 8a-c through Figures 8d-f and Figures 8g-i show the MPe net rate of progress of the most influential combustion chemical reactions considered in the previous paragraph. Referring to Figures 8a-i, the chain branching reaction R130: H + O_2 ⇔ O + OH, R134: H_2 + OH ⇔ H + H_2O, R146: CO + OH ⇔ CO_2 + H, and R151: HCO + M ⇔ CO + H + M have the highest net rate of progress. However, the chain branching reaction R130: H + O_2 ⇔ O + OH has the highest net rate of progress amidst these reactions. At the different equivalence ratios, the maximum net rate of progress of R130 is attained at the equivalence ratio of 1.0. The peak net rate of progress of R130 at ϕ of 0.7 is 5.20 kmol/m^3/s, ϕ of 1.0 is 12.50 kmol/m^3/s and ϕ of 1.4 is 7.14 kmol/m^3/s. Whereas the maximum net rate of progress of R130 occurs at the initial temperature of 483 K for the different initial temperatures, the maximum net rate of progress of R130 is attained at the initial pressure of 4 bar for the various initial pressures. The maximum

value of R130 at 423 K is 12.50 kmol/m^3/s, 453 K is 13.28 kmol/m^3/s and 483 K is 14.12 kmol/m^3/s. The maximum net rate of progress of R130 at 1 bar is 12.50 kmol/m^3/s, 2 bar is 39.29 kmol/m^3/s and 4 bar is 116.23 kmol/m^3/s.

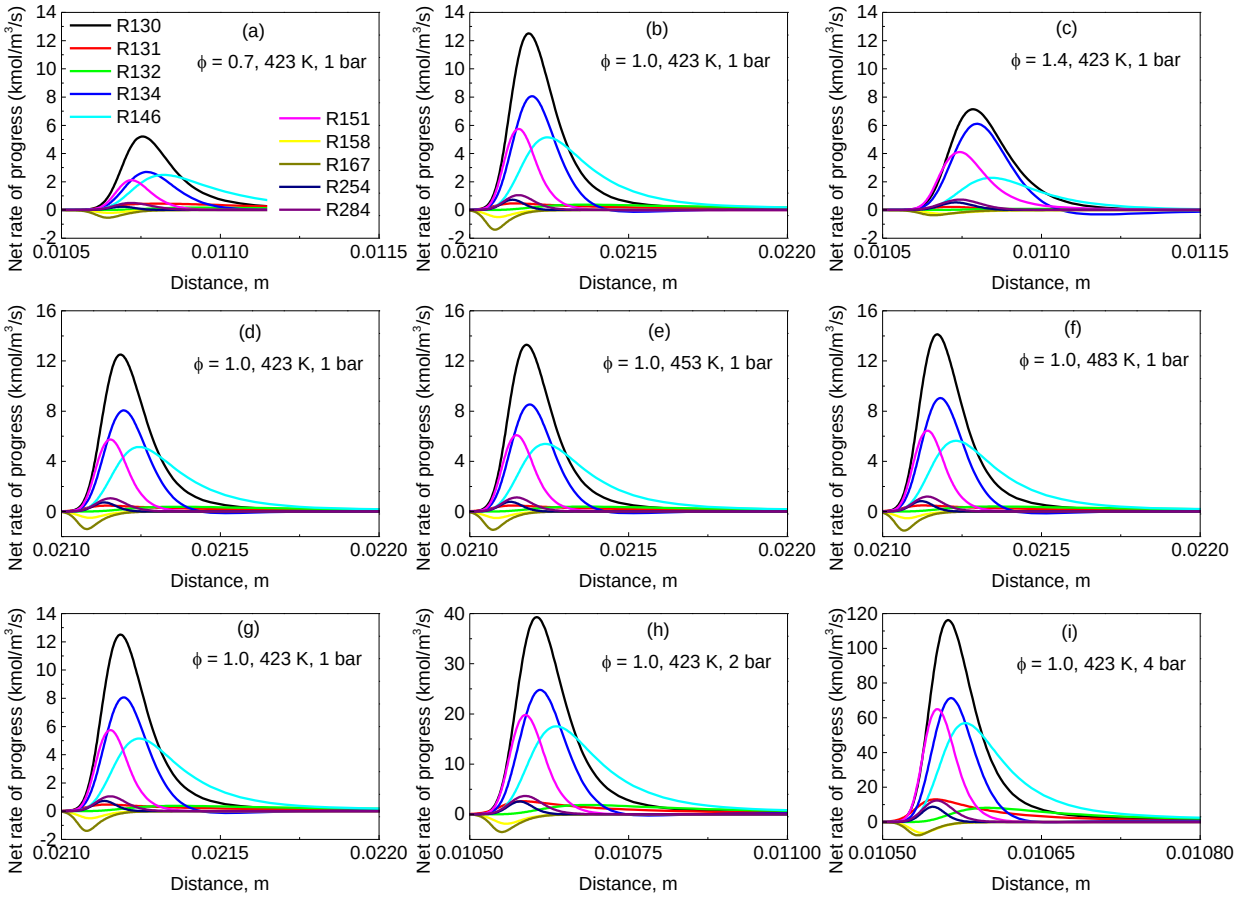


Figure 8. MPe net rate of progress of the most influential combustion reactions at different (a)-(c) equivalence ratios, (d)-(f) temperatures and (g)-(i) pressures.

Figures 9a-c depict the rate of production of MPe relevant combustion species at the equivalence ratios of 0.7, 1.0 and 1.4. Moreover, Figures 9d-f present the production rate at the initial temperatures of 423 K, 453 K and 483 K while Figures 9g-i plots the production rate at the initial pressures of 1 bar, 2 bar and 4 bar. From Figure 9, H_2O is produced in the largest quantity followed by the formation of CO and H_2. The peak value of H_2O at ϕ of 0.7 is 6.25 kmol/m^3/s, ϕ of 1.0 is 14.75 kmol/m^3/s and ϕ of 1.4 is 9.32 kmol/m^3/s. The peak value of H_2O at 423 K is 14.75 kmol/m^3/s, 453 K is 15.65 kmol/m^3/s and 483 K is 16.62 kmol/m^3/s. The maximum value of H_2O at 1 bar is 14.75 kmol/m^3/s, 2 bar is 47.97 kmol/m^3/s and 4 bar is 148.94 kmol/m^3/s. H_2O and CO_2 always have positive values, and

first increase and decrease after obtaining the peak value. On the other hand, O_2 and MPe invariably have negative production rates indicating that they are mainly consumed in the combustion process.

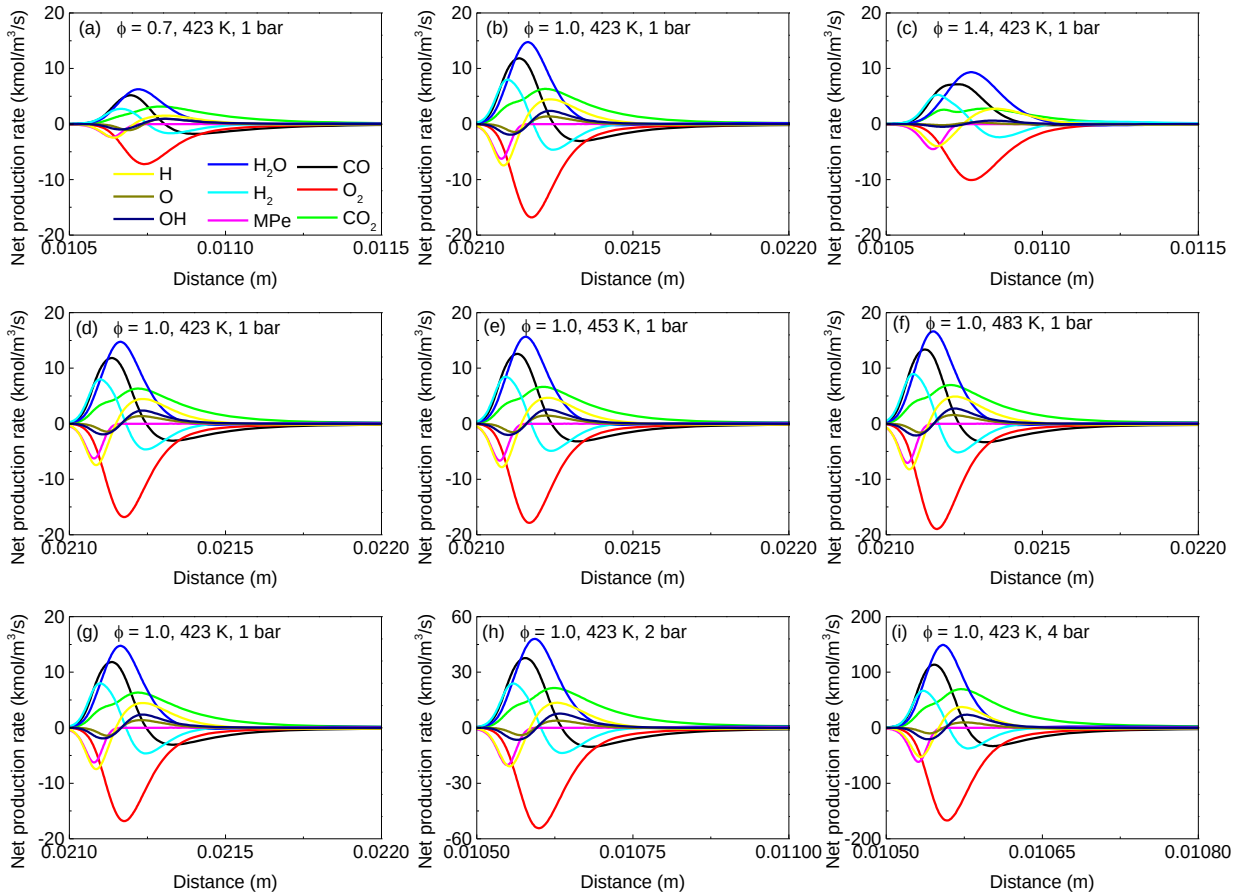


Figure 9. Production rate of species in MPe combustion at different (a)-(c) equivalence ratios, (d)-(f) temperatures and (g)-(i) pressures.

Figures 10a and b describe the reaction pathways of MPe at 423, 453 and 483 K and 1, 2, and 4 bar respectively. The main pathways for the decomposition of MPe are MPe→MPe2J→MPeMJ→MPe3J. Other secondary pathways for the decomposition of MPe are MPe→MPe5J and MPe→MPe4J→Me2J. Thus, the abstraction of an H atom leads to the formation of MPe radicals MPe2J, MPeMJ, MPe3J, MPe4J, and MPe5J. Moreover, MPe radicals like MPe2D and MPe3D are formed for the abstraction of two H atoms and the occurrence of double bonds. On the one hand, the main pathways for the conversion of MPe to carbon dioxide are MPe→MPe2J→MPeMJ→MPe3J→CH_3OCO→CO_2. Other relevant pathways are the conversion of MPe to CO, thus, MPe→MPe2J→MPeMJ→CH_2O→HCO→CO and MPe→MPe2J→MPeMJ→nC_4H_9CO→CO. Finally,

Figures 10a and b show that the flux at 483 K and 4 bar is higher than the fluxes at 423 K and 453 K and 1 and 2 bar. It is worth noting that the reaction pathway data were obtained at the maximum temperature gradient of the premixed flame. Moreover, elemental fluxes lower than 0.05 were not recorded.

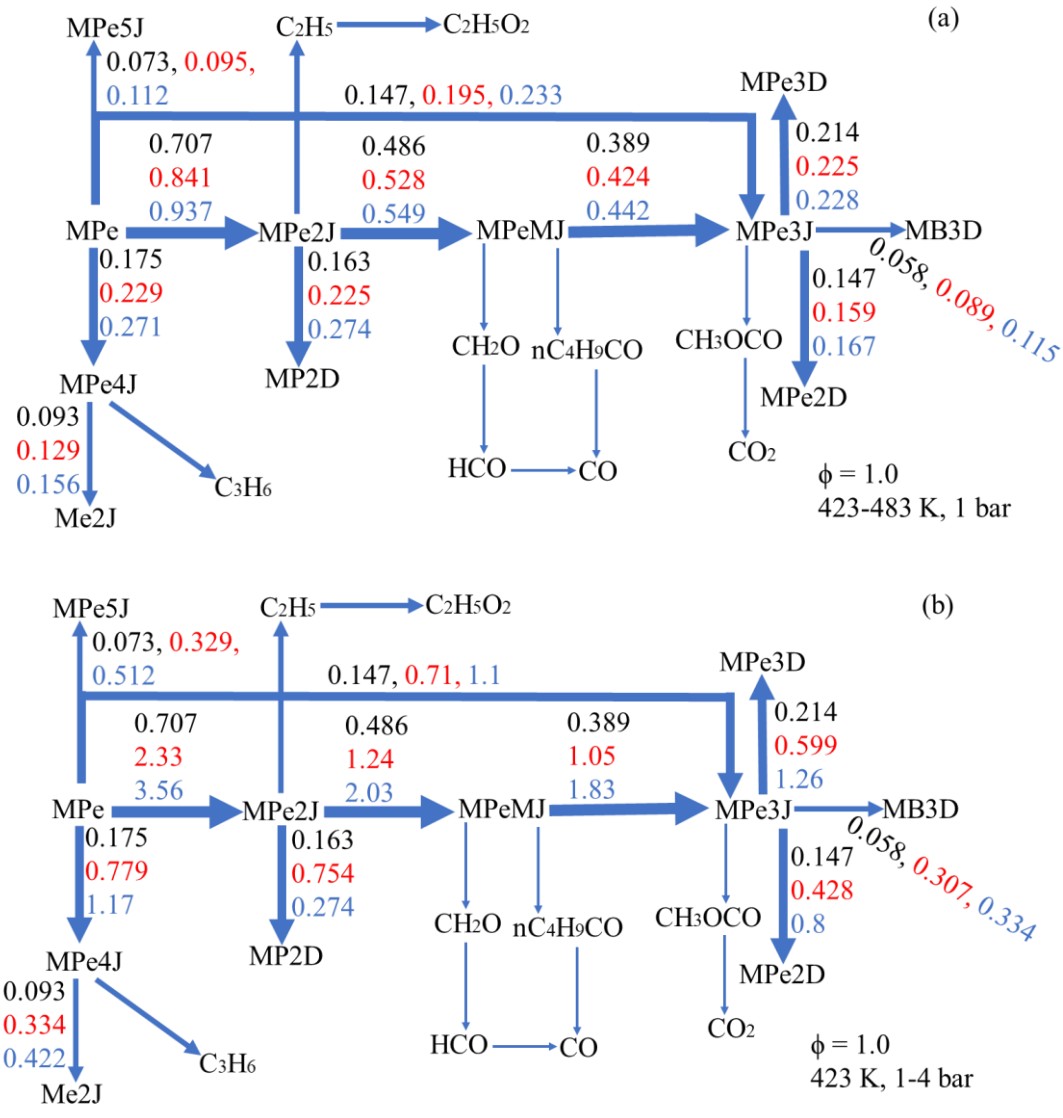


Figure 10. MPe/air mixtures reaction pathways at (a) different temperatures and (b) different pressures. Black: 423 K and 1 bar; Red: 453 K and 2 bar; Blue: 483 K and 4 bar represent the flux at the various initial temperatures and pressures respectively.

5. Conclusions

Renewable green fuels such as methyl pentanoate could be used to reduce carbon dioxide emissions into the atmosphere when adopted as a transportation fuel. Therefore, it is important to have a good understanding of its combustion characteristics for its potential application in combustion devices. In this regard, the combustion characteristics of MPe were investigated at the initial pressures of 1, 2 and 4 bar, initial temperatures of 423, 453 and 483 K and the equivalence ratios of 0.7-1.4 using numerical and experimental investigations.

The investigated combustion characteristics include the peak pressures, pressure rise rates, laminar burning velocity, reaction pathways, etc. of MPe. MPe peak pressures and pressure rise rates increased with increasing initial pressures and decreased with increasing initial temperatures. Also, the experimental laminar burning velocities agreed well with simulated laminar burning velocities. Empirical correlations were formulated to obtain MPe laminar burning velocities up to the initial pressures and temperatures of 8 bar and 573 K, respectively. MPe flame speed was highly accelerated by the reaction R130: $H + O_2 \Leftrightarrow O + OH$. Besides, the rate of progress of the reactions revealed that R130: $H + O_2 \Leftrightarrow O + OH$ increased MPe reactivity. The combustion species which was produced in larger quantity was H_2O. The main pathways for the decomposition of MPe were MPe→MPe2J→MPeMJ→MPe3J whereas the conversion of MPe to carbon dioxide was MPe→MPe2J→MPeMJ→MPe3J→CH_3OCO→CO_2.

In summary, this study laminar burning velocities could be used to validate and optimize newly developed and old MPe chemical mechanisms. The laminar burning velocities, peak pressures and pressure rise rates results could be beneficial to engine research engineers, fire safety engineers and the combustion community to design new or modify existing engines for methyl pentanoate and devise safety measures and standards for MPe. MPe ignition delay time, flame instability and chemical mechanism will be thoroughly investigated in future studies.

Acknowledgements

The support from the National Key R&D Program of China (2018YFB1501405), Ningbo Major Science and Technology Project (20212ZDYF020041), Open Project of the State Key Laboratory of Clean Energy Utilization, Zhejiang University (ZJU-CEU2020001), and the China Postdoctoral Foundation is much appreciated. Thanks to Mr Qiyang Wang and Mr Liu Kai for helping in the experimental work.

References

[1] S. Douvartzides, N.D. Charisiou, W. Wang, V.G. Papadakis, K. Polychronopoulou, M.A. Goula, Catalytic fast pyrolysis of agricultural residues and dedicated energy crops for the production of high energy density transportation biofuels. Part I: Chemical pathways and bio-oil upgrading, Renew. Energy. 185 (2022) 483–505. https://doi.org/10.1016/j.renene.2021.12.083.

[2] L. Moretti, M. Milani, G.G. Lozza, G. Manzolini, A detailed MILP formulation for the optimal design of advanced biofuel supply chains, Renew. Energy. 171 (2021) 159–175. https://doi.org/10.1016/j.renene.2021.02.043.

[3] R. Yazdanparast, F. Jolai, M.S. Pishvaee, A. Keramati, A resilient drop-in biofuel supply chain integrated with existing petroleum infrastructure: Toward more sustainable transport fuel solutions, Renew. Energy. 184 (2022) 799–819. https://doi.org/10.1016/j.renene.2021.11.081.

[4] Y. Kuwahara, Y. Magatani, H. Yamashita, Ru nanoparticles confined in Zr-containing spherical mesoporous silica containers for hydrogenation of levulinic acid and its esters into γ-valerolactone at ambient conditions, Catal. Today. 258 (2015) 262–269. https://doi.org/10.1016/j.cattod.2015.01.015.

[5] A.M. Dmitriev, K.N. Osipova, D.A. Knyazkov, I.E. Gerasimov, A.G. Shmakov, O.P. Korobeinichev, Comparative analysis of the chemical structure of ethyl butanoate and methyl pentanoate flames, Combust. Explos. Shock Waves. 54 (2018) 125–135. https://doi.org/10.1134/S0010508218020016.

[6] Z. Yu, X. Lu, C. Liu, Y. Han, N. Ji, Synthesis of γ-valerolactone from different biomass-derived feedstocks: Recent advances on reaction mechanisms and catalytic systems, Renew. Sustain. Energy Rev. 112 (2019) 140–157. https://doi.org/10.1016/j.rser.2019.05.039.

[7] H. Guo, Y. Hiraga, X. Qi, R.L. Smith, Hydrogen gas-free processes for single-step preparation of transition-metal bifunctional catalysts and one-pot Γ-valerolactone synthesis in supercritical CO2 -ionic liquid systems, J. Supercrit. Fluids. 147 (2019) 263–270. https://doi.org/10.1016/j.supflu.2018.11.010.

[8] F. Contino, P. Dagaut, F. Halter, J.B. Masurier, G. Dayma, C. Mounaïm-Rousselle, F. Foucher, Screening method for fuels in homogeneous charge compression ignition engines: Application to valeric biofuels, Energy and Fuels. 31 (2017) 607–614. https://doi.org/10.1021/acs.energyfuels.6b02300.

[9] F. Contino, F. Foucher, F. Halter, G. Dayma, P. Dagaut, C. Mounaïm-Rousselle, Engine performances and emissions of second-generation biofuels in spark ignition engines: The case of methyl and ethyl valerates, SAE Tech. Pap. 6 (2013) 1–6. https://doi.org/10.4271/2013-24-0098.

[10] O.P. Korobeinichev, I.E. Gerasimov, D.A. Knyazkov, A.G. Shmakov, T.A. Bolshova, N. Hansen, C.K. Westbrook, G. Dayma, B. Yang, An experimental and kinetic modeling study of premixed laminar flames of methyl pentanoate and methyl hexanoate, Zeitschrift Fur Phys. Chemie. 229 (2015) 759–780. https://doi.org/10.1515/zpch-2014-0596.

[11] I.E. Gerasimov, T.A. Bolshova, I.A. Zaev, A. V. Lebedev, B. V. Potapkin, A.G. Shmakov, O.P. Korobeinichev, Reduced chemical kinetic mechanism for methyl pentanoate combustion, Energy and Fuels. 31 (2017) 14129–14137. https://doi.org/10.1021/acs.energyfuels.7b01907.

[12] B.W. Weber, J.A. Bunnell, K. Kumar, C.J. Sung, Experiments and modeling of the autoignition of methyl pentanoate at low to intermediate temperatures and elevated pressures in a rapid compression machine, Fuel. 212 (2018) 479–486. https://doi.org/10.1016/j.fuel.2017.10.037.

[13] P. Lu, Y. Gou, J. He, P. Li, C. Zhang, X. Li, Shock tube study of methyl pentanoate ignition at high temperatures, Acta Phys. - Chim. Sin. 34 (2018) 618–624. https://doi.org/10.3866/PKU.WHXB201710252.

[14] D.A. Knyazkov, T.A. Bolshova, A.M. Dmitriev, A.G. Shmakov, O.P. Korobeinichev, The effect of methyl pentanoate addition on the structure of a non-premixed counterflow n-heptane/O2 flame, Energy and Fuels. 32 (2018) 2397–2406. https://doi.org/10.1021/acs.energyfuels.7b03185.

[15] Y. Shang, H. Ning, J. Shi, S.N. Luo, Kinetic modeling of methyl pentanoate pyrolysis based on: Ab initio calculations, Phys. Chem. Chem. Phys. 22 (2020) 17978–17986. https://doi.org/10.1039/d0cp02821e.

[16] F. Oppong, L. Zhongyang, X. Li, C. Xu, Investigations on laminar premixed flame characteristics of ethyl acetate, Combust. Flame. 230 (2021) 111454. https://doi.org/10.1016/j.combustflame.2021.111454.

[17] G.P. Oliveira, M.E. Sbampato, C.A. Martins, L.R. Santos, L.G. Barreta, R.F. Boschi Gonçalves, Experimental laminar burning velocity of syngas from fixed-bed downdraft biomass gasifiers, Renew. Energy. 153 (2020) 1251–1260. https://doi.org/10.1016/j.renene.2020.02.083.

[18] P. Xiao, C. fon Lee, H. Wu, F. Liu, Effects of hydrogen addition on the laminar methanol-air flame under different initial temperatures, Renew. Energy. 154 (2020) 209–222. https://doi.org/10.1016/j.renene.2020.03.037.

[19] F. Oppong, C. Xu, X. Li, L. Zhongyang, Laminar flame characteristics of 2-ethylfuran/air mixtures: Experimental and kinetic modelling investigations, Fuel. 307 (2022) 121785. https://doi.org/10.1016/j.fuel.2021.121785.

[20] C. Xu, H. Wang, F. Oppong, X. Li, K. Zhou, W. Zhou, S. Wu, C. Wang, Determination of laminar burning characteristics of a surrogate for a pyrolysis fuel using constant volume method, Energy. 190 (2020) 116315. https://doi.org/10.1016/j.energy.2019.116315.

[21] D.G. Goodwin, H.K. Moffat, R.L. Speth, Cantera: An Object-oriented Software Toolkit for Chemical Kinetics, Thermodynamics, and Transport Processes., (2017). https://doi.org/10.5281/zenodo.170284.

[22] C.C.M. Luijten, E. Doosje, L.P.H. de Goey, Accurate analytical models for fractional pressure rise in constant volume combustion, Int. J. Therm. Sci. 48 (2009) 1213–1222. https://doi.org/10.1016/j.ijthermalsci.2008.12.020.

[23] M. Faghih, Z. Chen, The constant-volume propagating spherical flame method for laminar flame speed measurement, Sci. Bull. 61 (2016) 1296–1310. https://doi.org/10.1007/s11434-016-1143-6.

[24] D. Razus, V. Brinzea, M. Mitu, C. Movileanu, D. Oancea, Burning velocity of propane-air mixtures from pressure-time records during explosions in a closed spherical vessel, Energy and Fuels. 26 (2012) 901–909. https://doi.org/10.1021/ef201561r.

[25] Z. Chen, M.P. Burke, Y. Ju, Effects of compression and stretch on the determination of laminar flame speeds using propagating spherical flames, Combust. Theory Model. 13 (2009) 343–364. https://doi.org/10.1080/13647830802632192.

[26] G. Cui, S. Wang, J. Liu, Z. Bi, Z. Li, Explosion characteristics of a methane/air mixture at low initial temperatures, Fuel. 234 (2018) 886–893. https://doi.org/10.1016/j.fuel.2018.07.139.

[27] Q. Li, Y. Cheng, Z. Huang, Comparative assessment of the explosion characteristics of alcohol-air mixtures, J. Loss Prev. Process Ind. 37 (2015) 91–100. https://doi.org/10.1016/j.jlp.2015.07.003.

[28] B. Zhang, G. Xiu, C. Bai, Explosion characteristics of argon/nitrogen diluted natural gas-air mixtures, Fuel. 124 (2014) 125–132. https://doi.org/10.1016/j.fuel.2014.01.090.

[29] L. Zhang, H. Ma, Z. Shen, L. Wang, R. Liu, J. Pan, Influence of pressure and temperature on explosion characteristics of n-hexane/air mixtures, Exp. Therm. Fluid Sci. 102 (2019) 52–60. https://doi.org/10.1016/j.expthermflusci.2018.11.004.

[30] C. Tang, Z. Huang, C. Jin, J. He, J. Wang, X. Wang, H. Miao, Explosion characteristics of hydrogen-nitrogen-air mixtures at elevated pressures and temperatures, Int. J. Hydrogen Energy. 34 (2009) 554–561. https://doi.org/10.1016/j.ijhydene.2008.10.028.

[31] F. Oppong, C. Xu, L. Zhongyang, X. Li, W. Zhou, C. Wang, Evaluation of explosion characteristics of 2-methylfuran/air mixture, J. Loss Prev. Process Ind. 62 (2019) 103954. https://doi.org/10.1016/j.jlp.2019.103954.

[32] F. Oppong, C. Xu, L. Zhongyang, X. Li, W. Zhou, W. Siyuan, J. Zhou, Investigating the explosion of ethyl acetate in the presence of hydrogen, Int. J. Hydrogen Energy. 45 (2020) 20400–20407. https://doi.org/10.1016/j.ijhydene.2019.12.136.

[33] E. Hu, Z. Xu, Z. Gao, J. Xu, Z. Huang, Experimental and numerical study on laminar burning velocity of gasoline and gasoline surrogates, Fuel. 256 (2019) 115933. https://doi.org/10.1016/j.fuel.2019.115933.

[34] G. Broustail, F. Halter, P. Seers, G. Moréac, C. Mounaïm-Rousselle, Experimental determination of laminar burning velocity for butanol/iso-octane and ethanol/iso-octane blends for different initial pressures, Fuel. 106 (2013) 310–317. https://doi.org/10.1016/j.fuel.2012.10.066.

[35] G. Wang, Y. Li, W. Yuan, Y. Wang, Z. Zhou, Y. Liu, J. Cai, Investigation on laminar flame propagation of n-butanol/air and n-butanol/O2/He mixtures at pressures up to 20 atm, Combust. Flame. 191 (2018) 368–380. https://doi.org/10.1016/j.combustflame.2018.01.025.

[36] C.K. Law, Combustion Physics, Cambridge University Press, 2006.

[37] Stephen R Turns, An introduction to combustion : Concepts and applications, Third Edit, McGraw Hill, 2012. https://doi.org/10.1017/CBO9781107415324.004.

[38] I. Glassman, R.A. Yetter, N.G. Glumac, Combustion, Fifth Edit, Elsevier Ltd, 2015.